Development of 1 kHz, few-cycle, mJ level CEP stabilized laser source

6.1 Introduction

In this chapter I present the development of a laser system (Salle Noire) delivering CEP stabilized, 1 mJ, few-cycle pulses at 1 kHz repetition rate. In order to generate such pulses, a multi-mJ, CEP-stable front-end laser system, providing relatively short pulse duration (sub-30 fs), is necessary due to the current limitations of post-compression techniques used to get into the few-cycle regime (section 6.11). The high energy few-cycle pulses can then be used to drive attosecond pulse generation on solid target. At the beginning of my Ph.D there were no commercially available systems having the required characteristics. In particular the CEP stabilization was guaranteed for pulses with an energy lower than 1 mJ. Achieving a long term stabilization of the CEP at the multi-mJ level imposes various constraints on the design of laser system. Furthermore we wanted to build a laser source with a simple and robust architecture for daily operation.
The chosen configuration was:

- a broadband oscillator, CEP stabilized
- a stretcher composed of a block of glass and an AOPDF
- a first commercial mJ amplifier
- a second home-made amplifier for boosting the energy up to several mJ
- a hybrid compressor (prisms + chirped mirrors) or (transmission gratings + chirped mirrors)
- a hollow fiber for the compression down to the few-cycle regime
- a commercial device for stabilizing CEP at the kHz repetition rate.

We decided not to build the oscillator and the first amplification stage. The purchased front-end is a Femtopower Compact Pro CEP (Femtolasers GmbH) commercial system. This system delivers 1 kHz, CEP stabilized pulses with a temporal duration < 30 fs and a compressed energy of 1 mJ. The CEP is stabilized with a commercial stabilizing device (Menlo-system GmbH). We modified the system to accommodate an AOPDF pulse shaper between passes 4 and 5 to control dynamically the spectral phase of the system. The output of this first amplifier is injected into a home made three-pass amplifier boosting the energy up to the multi-mJ level. A single pump laser is used for pumping both amplification stages. The pulses are finally compressed in a hybrid compressor. The first configuration we tested was a combination of a prism compressor and chirped mirrors. Although pulses as short as 22 fs with an energy of 4 mJ was obtained with this configuration, we observed a substantial degradation of the spatial profile after compression due to inhomogeneities in the prisms. Furthermore CEP measurement of the output pulses has underlined the impossibility in achieving CEP stabilization in this configuration. For these reasons we tested a second hybrid compression scheme using a transmission gratings compressor and chirped mirrors. In this configuration we obtain daily 25 fs, 2.2 mJ, CEP stabilized pulses.

6.2 22 fs, 4 mJ 1 kHz source

I will now review more specifically the main components of the laser source starting with the configuration using the prism compressor and chirped mirrors.

6.2.1 CEP stabilized oscillator

The oscillator is a Kerr lens mode locking Rainbow CEP type (femtolasers GmbH) [1]. It delivers pulses with an energy of 2.5 nJ at a repetition of 80 MHz. The schematic of the cavity is presented in Fig. 6.1. The spectrum emitted by the oscillator is shown in Fig. 6.2. The FWHM is 220 nm corresponding to a transform limited duration of 6.8 fs. A nonlinear interferometer is implemented after the oscillator for the stabilization of the CEP with a fast loop. The pulses are focused with a concave mirror in a PPLN (Periodically Poled Lithium Niobate) crystal. The intensity in the crystal is high enough to broaden the spectrum by SPM and to generate intra-pulse difference frequency generation (DFG) between the high frequency and low frequency part of the spectrum [2]. Interference between lower frequencies of the fundamental spectrum and the difference frequency signal yields a beating at the frequency f_{ceo}. This signal is directed with a dichroic mirror to a frequency meter and a feedback electronic loop for the stabilization of the CEP (section 2.2.1). When the feedback loop is activated the electronic part of the stabilizing system controls an acousto-optic modulator that modulates the pump power of the oscillator. The resulting variation in intensity of the pulse inside the cavity forces f_{ceo} to be equal to $f_{rep}/4$. Forcing the two signals to oscillate in phase gives $\Delta\varphi_0 = 2\pi/4$, so that every 4 pulses exiting the cavity have identical CEP φ_0. For the correct operation of the system the frequency f_{ceo} must be detected with a signal to noise ratio (SNR) higher than 30 dB.

The oscillator pulses then go through an optical isolator and are stretched in a 20 cm block of glass (SF7).

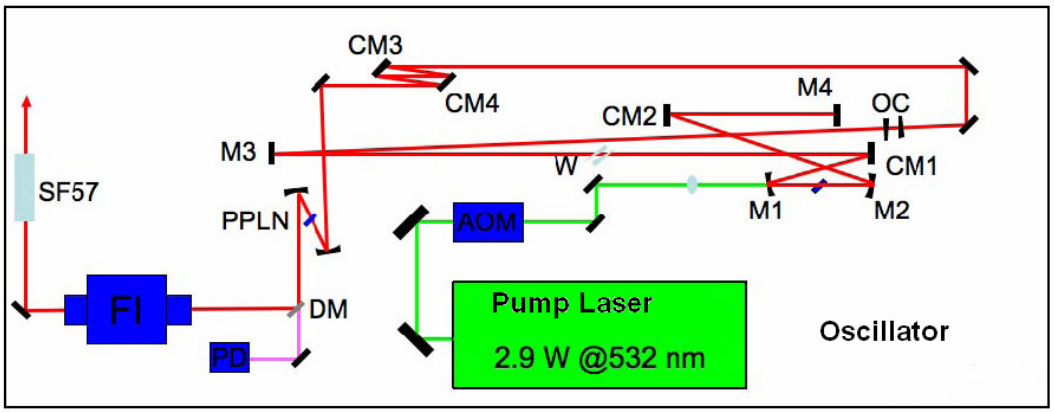

Figure 6.1: Schematic of the Rainbow CEP (Femtolasers GmbH). M1-M2 sub-cavity mirrors. CM1-CM2 chirped mirrors for the compensation of the intra-cavity GVD.

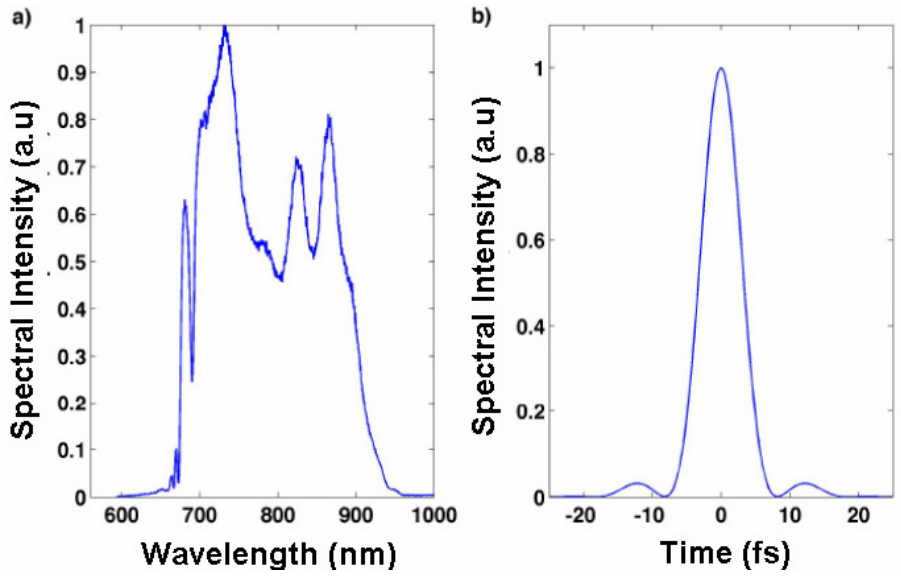

Figure 6.2: (a) Output spectrum of the oscillator (FWHM 220 nm), (b) corresponding Fourier transform temporal profile (temporal duration 6.8 fs).

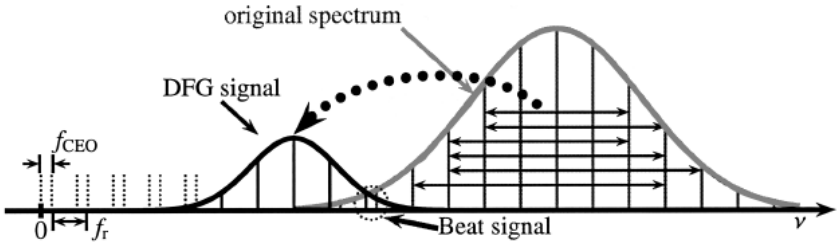

Figure 6.3: Schematic of the principle for the generation of the beat signal at the frequency f_{CEO} with a device using the difference frequency generation in a PPLN crystal. The pulse is focused in the crystal. new spectral components are generated by SPM. In this crystal there is a nonlinear process of difference frequency generation (DFG) between the high frequency and low frequency part of the spectrum [2]. Interference between low frequency of the fundamental spectrum and the DF signal yields a beating at the frequency f_{ceo}

6.2.2 Multi-pass amplifier

The commercial multi-pass amplifier (10 passes) delivers pulses with an energy of 2 mJ at 1 kHz (Fig. 6.4). The pump laser is a Nd:YLF (PI, Photonics Industries) delivering 1 kHz, 50 mJ (50 W) pulses at 527 nm. Only 11 W are used for pumping this amplification stage. In the first 8 passes the energy goes from few nJ to 400 μJ. After the fourth pass the beam goes through the AOPDF (HR800) and a Pockels cell for the selection of a train of pulses at 1 kHz. These pulses are further amplified to an energy of 2 mJ. The ASE level estimated by blocking the injection in the amplifier is around 40 μJ. The choice of the location of the AOPDF in the amplifier is original. We chose this configuration because, due to the gain narrowing in the first 4 passes, the spectral bandwidth injected into the the AOPDF is reduced compared to the case where it is placed after the oscillator. As a consequence, the diffraction efficiency of the AOPDF is higher, and thus the pulses can be amplified to the mJ level in the following passes while maintaining a good temporal contrast (10^8 at the output of the Femtopower).

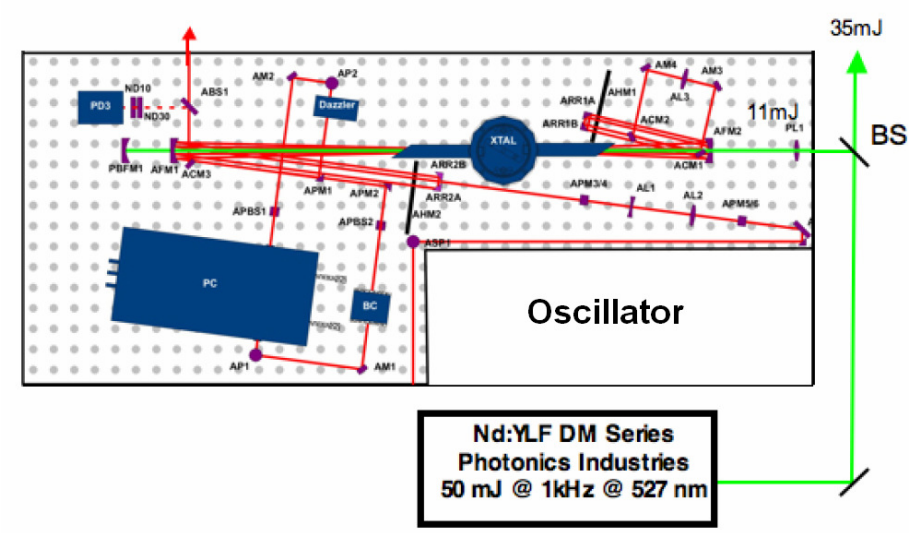

Figure 6.4: Schematic of the commercial amplification system. It is a ten-pass amplifier with an output pulse energy of 2 mJ at 1 kHz repetition rate(uncompressed). The crystal is pumped with 11 W (at 527 nm) and cooled at 193 K with a cryostat (XTAL). The Dazzler and the pockels cell are placed after the fourth pass.

6.2.3 AOPDF (Dazzler)

During all my Ph.D I used several times the AOPDF [3] for the pulse shaping and characterization. I give here a brief introduction of this device. It is constituted of a TeO_2 crystal which is optically and acoustically birefringent. An acoustic wave is launched by a transducer excited by an electronic signal. The acoustic wave propagates with a velocity V along the z axis and hence reproduces spatially the temporal shape of the rf signal. Two optical polarization modes can be coupled efficiently by the acousto-optic interaction only when some phase matching condition is achieved. If there is locally only one spatial frequency in the acoustic grating, then only one optical frequency can be diffracted at a position along z. The incident optical short pulse is initially in mode 1. Every frequency ω travels a certain distance before it encounters a phase-matched spatial frequency of the acoustic wave. At this position z(ω), part of the energy is diffracted into mode 2. The pulse leaving the device in mode 2 will be made up of all the spectral components that have been diffracted at various positions z(ω). Since the velocities of the modes are different, each frequency will experience a different time delay. The amplitude of the output pulse, or diffraction efficiency, is controlled by the acoustic power at position z(ω). The optical output $E_{out}(t)$ of the AOPDF is a function of the optical input $E_{in}(t)$ and of the electric signal H(t). More precisely, it has been shown to be proportional to the convolution of the optical input and the scaled electric field:

$$E_{out}(t) \propto E_{in}(t) \otimes H(t/\alpha) \tag{6.1}$$

where the scaling factor, $\alpha = \Delta n(V/c)$, is the ratio of the speed of sound to the speed of light times the index difference between the ordinary and extraordinary polarizations. α is the ratio of the acoustic frequency. Relation (6.1) can be written in the frequency domain as:

$$\tilde{E}_{out}(\omega) \propto \tilde{E}_{in}(\omega)H(\alpha\omega) \tag{6.2}$$

In this formulation H(t/α) appears as the impulse response of a filter applied to the input optical pulse. By generating a proper function S(t) one can achieve any arbitrary convolution with a temporal resolution given by the inverse of the available filter bandwidth.

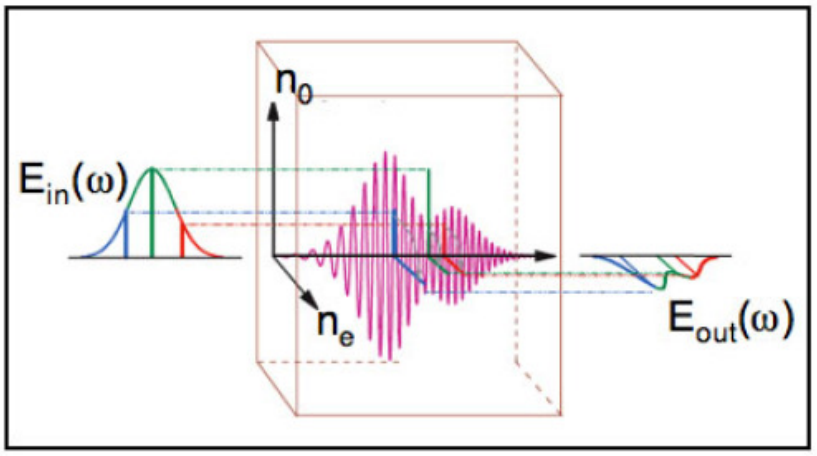

Figure 6.5: Schematic representation of the Acousto-Optic Dispersive Programmable Filter

6.2.4 Home made amplifier

The second amplifier is a home made three-pass amplifier. A schematic of this amplifier is shown in Fig. 6.6. The Ti:Sa crystal, cut at Brewster angle, is under vacuum and cooled at 195 K. The pump beam is down collimated by a (3:1) telescope and is then focused with a lens (L2) on the crystal. The power of the pump is 25 W. The absorbtion of the crystal is 75 % and the transmitted beam is refocused with a concave mirror (M1). The injection beam passes through an optical isolator to avoid any return into the first amplifier. A mirror telescope and a focusing lens (L1) are used to achieve the correct beam size on the crystal. After each pass the beam is re-imaged using concave dielectric mirrors (M2-M3) in order to have for each pass the correct beam size on the crystal. The diameter at $1/e^2$ in intensity of the infrared beam is roughly 1 mm for each pass. The geometrical focus for each pass is located before the crystal to have a slightly divergent beam to compensate the thermal lens in the crystal. The beam focus is inside the vacuum chamber to avoid any nonlinear effects in air. The output energy is 6 mJ. The total gain of the amplifier is 7.5.

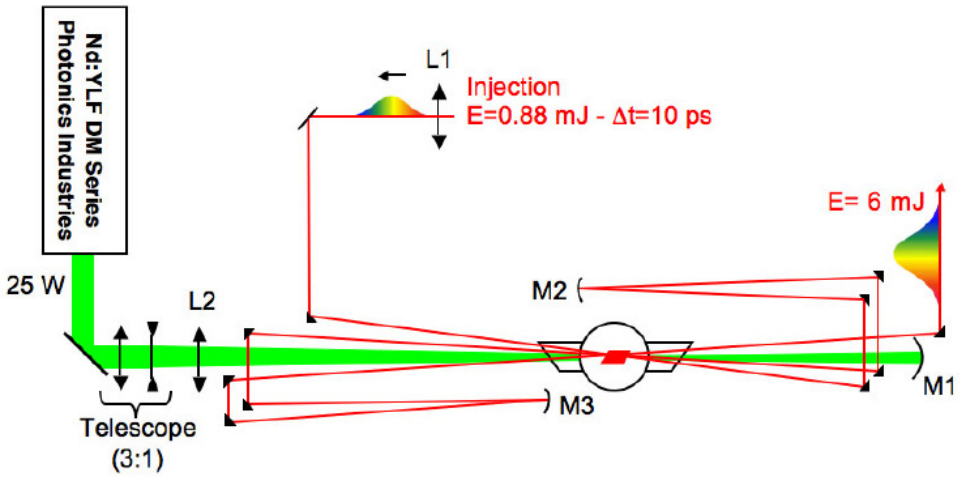

Figure 6.6: Schematic of the home made amplifier. L1:converging lens f=1500 mm. L2:converging lens f=700 mm. M1: dielectric mirror treated for 527 nm

The number of passes in this amplifier is limited to three due to the high B integral value (1.35 rad). This value needs to be added to the 3.5 radians already accumulated in the first amplifier. A total B integral higher than 4 radians is typically considered too high for the correct functioning of a CPA laser. As shown in the next section, the DazScope technique enables to measure and pre-compensate this nonlinear phase and therefore to achieve near perfectly compressed pulses. The high B integral of this chain originates from the small pulse stretching (10 ps). This choice is motivated by the fact that a small stretching factor enables the use of prism or very compact gratings compressors with increased insensitivity to dispersion fluctuations. This is of fundamental importance for achieving a good CEP stability.

6.2.5 Hybrid compressor: prism + chirped mirrors

The calculations for the design of the prism compressor were made by A. Trisorio from the PCO group. The values of dispersion added by this compressor are shown in Tab.1 together with the overall dispersion of the laser system Tab.2. The picture of the prisms and a schematic of the prism compressor are shown in Fig. 6.9 and Fig. 6.10

Incidence angle	d	λ_0	$\Delta\lambda$	$\varphi^2(\omega)$ fs^2	$\varphi^3(\omega)$ fs^3	$\varphi^4(\omega)$ f4
55.6°	30 mm	800 nm	750-850 nm	-64090	-95760	-262710

Figure 6.7: Parameter and dispersion introduced by the prisms

Optical elements	$\varphi^2(\omega)$ (fs^2)	$\varphi^3(\omega)$ (fs^3)	$\varphi^4(\omega)$ (fs^4)
Stretcher (20 cm of glass type SF57)	44206	31000	6730
Faraday isolator	5291	2693	-12
Pockels cell + Polarizers	2473	1478	810
Ti: saphir crystal (10*8 mm)	4853	3360	-1245
Dazzler (crystal dispersion of 45 mm)	22320	14580	8955
Dazzler (dispersion added by the acoustic-wave)	-17000	30000	200000
Calcite Polarizers type CVI CPAS (3*19.4 mm)	2270	1222	-58
Faraday rotator	3854	1895	352
silica lenses	782	552	-211
Ti: saphir crystal (10*8 mm))	1441	1008	-373
TOTAL	**70490**	**91064**	**214954**

Figure 6.8: Dispersion introduced by the different elements of the laser chain. This dispersion corresponds to 10 ps stretched pulses

Figure 6.9: Picture of the prisms used in the hybrid compressor.

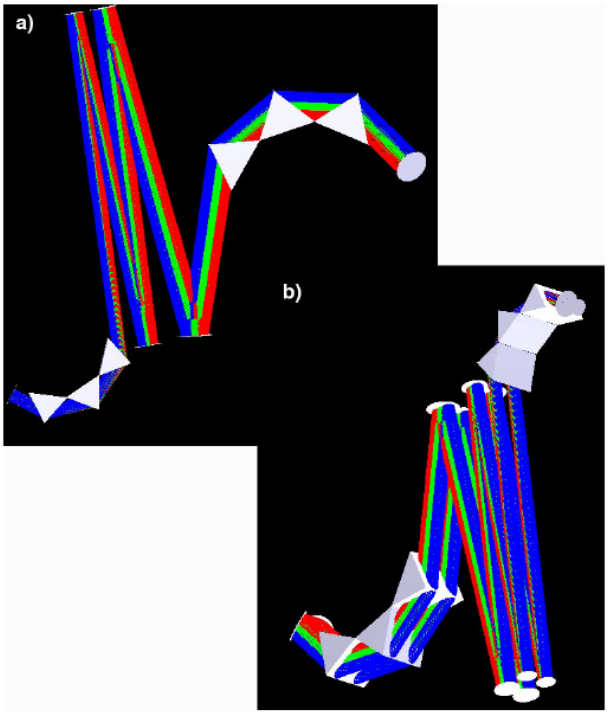

Figure 6.10: 3 D modeling of the prism compressor with Zeemax.

To limit SPM in the last prism, the temporal compression is ended by 32 reflections on two negatively dispersive chirped mirrors (Fig. 6.11). The characteristics of these chirped mirrors are:

- reflectivity higher than 99.5 % for a spectral range between 760 and 840 nm
- a damage threshold of 400 mJ/cm^2

- a second order dispersion of -200 fs^2 per bound with an angle of incidence of 15°

The pulse duration after the prism compressor is roughly 1 ps and is reduced to 22 fs after the 32 reflections (The total dispersion introduced by the chirped mirrors is -6400 fs^2).

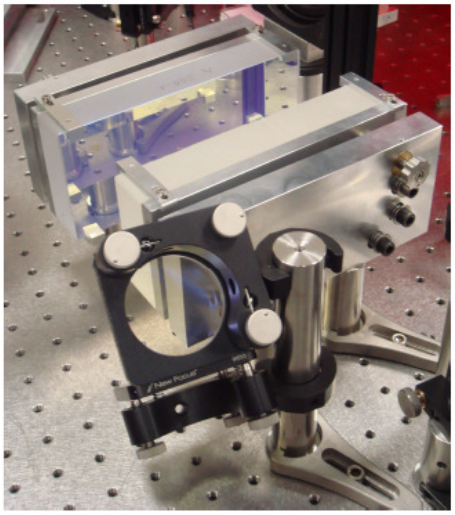

Figure 6.11: Photos of the chirped mirrors used in the hybrid compressor. The pulses are reflected 32 times on the mirrors to end the compression

The temporal duration has been optimized using a closed feedback loop (Dazscope), that is presented in the next section, and measured with a home made SPIDER. The compressed pulse energy is 4 mJ with an efficiency of the compressor of 67 %. The temporal contrast has also been measured in order to access the temporal quality of the pulses. This is shown in Fig. 6.12. The contrast is $5 * 10^5$ at a delay of 3 ps and $3 * 10^7$ for a delay of 15 ps. The ASE level is 10^7 at 40 ps. With a fast photodiode and a digital oscilloscope we measured the energy stability of the output pulses. The standard deviation of the energy fluctuations is 2.6 % over 10 minutes. This is due to the fact that the second amplifier is not saturated.
To test the quality of the beam we measured with a CMOS camera the far field spatial profile (f=1.5 m) at different z positions on either sides of the beam waist. From this measurement the M^2 factor can be calculated. In particular we obtain $M_x^2 = 1.9$ for the x axis and $M_y^2 = 2$ for the y axis. The spatial quality is not excellent and this is due to the relatively high B integral of our laser and to degradation of the spatial profile in the prism compressor. This is not too problematic because the spatial profile is cleaned with the propagation in the hollow-core fiber. Pre-compensation of nonlinear spectral phase with the pulse shaper and spatial cleaning in the hollow fiber enable us to avoid the main problems of a high B integral.

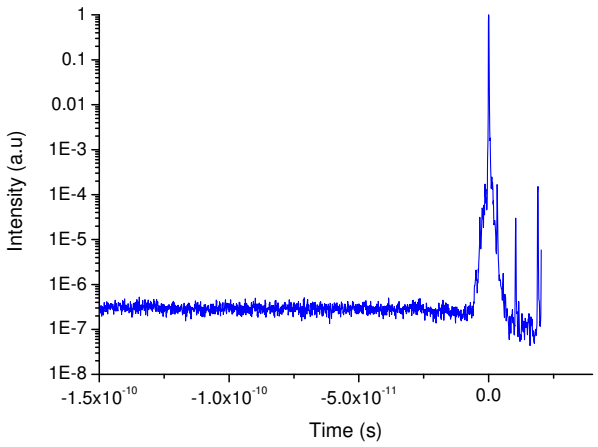

Figure 6.12: High dynamic range third order correlation (Sequoia, Amplitude Technologies) measurement of the pulses compressed in the hybrid compressor (prisms+chirped mirrors).The contrast is $5 * 10^5$ for a delay of 3 ps and $5 * 10^7$ for a delay of 15 ps.

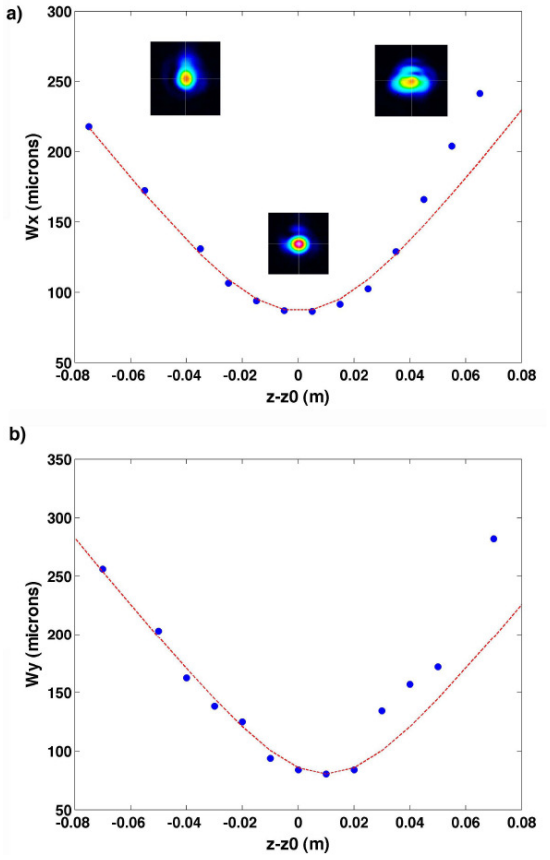

Figure 6.13: Measurement of the intensity profile focused with a f=1.5 m concave mirror for different position before and after the waist. (a) Radius at $1/e^2$, W_x in intensity measured along the x axis and fitting curve from the formula. (b) Radius at $1/e^2$, W_y in intensity measured along the y axis and fitting curve from the formula.

Bibliography

[1] T. Fuji, A. Unterhuber, V.S. Yakovlev, G. Tempea, A. Stingl, F. Krausz, and W. Drexler. Generation of smooth, ultra-broadband spectra directly from a prism-less ti:sapphire laser. *Applied Physics B: Lasers and Optics*, 77(1):125–128, August 2003.

[2] T. Fuji, A. Apolonski, and F. Krausz. Self-stabilization of carrier-envelope offset phase by use of difference-frequency generation. *Opt. Lett.*, 29(6):632–634, 2004.

[3] F. Verluise, V. Laude, Z. Cheng, Ch. Spielmann, and P. Tournois. Amplitude and phase control of ultrashort pulses by use of an acousto-optic programmable dispersive filter: pulse compression and shaping. *Opt. Lett.*, 25(8):575–577, 2000.

6.3 DazScope

6.3.1 Introduction

In this chapter I present the local spectral compression technique for the closed-loop optimization of the temporal duration, commercialized under the name DazScope™. I developed this technique in collaboration with FASTLITE. The starting point of this development was the study of the effect of the spectral phase on the XPW generation presented in section 4.6. From the results presented in this section there is a clear correlation between the shape of the XPW spectrum and the spectral phase of the input pulse. In particular, I have shown how the combination of second and third order spectral phase shifts the barycenter of the spectrum generated by the nonlinear process. This is even more evident using second harmonic generation (SHG) as the nonlinear effect. Fig. 6.14 shows for example the evolution of the SH spectrum function of $\varphi^{(2)}$ (x axis $\pm 2500 fs^2$) for different fixed values of $\varphi^{(3)}$ ($\pm 35000 fs^3$). The first figure on the left of the first line (figure 1) corresponds to $\varphi^{(3)} = -35000 fs^3$. The second figure of this line (figure 2) corresponds to $\varphi^{(3)} = -30625 fs^3$. The last figure on the right of the last line (figure 16) corresponds to $\varphi^{(3)} = 35000 fs^3$. From the different scans it is easy to see that the third order spectral phase passes through $\varphi^{(3)} = 0$ between picture 8 and 9 (respectively last figure of the second line and first figure of the third line) where the barycenter function of $\varphi^{(2)}$ changes the sign of the slope. For a single scan there is an absolute maximum of the SHG energy when $\varphi^{(2)} = 0$. Starting with this consideration it is important to see if, looking at the spectrum generated in the nonlinear process for different values of an added $\varphi^{(2)}$, enables the extraction of the spectral phase of the input pulses. This is demonstrated theoretically in the next section. The experimental results are then presented.

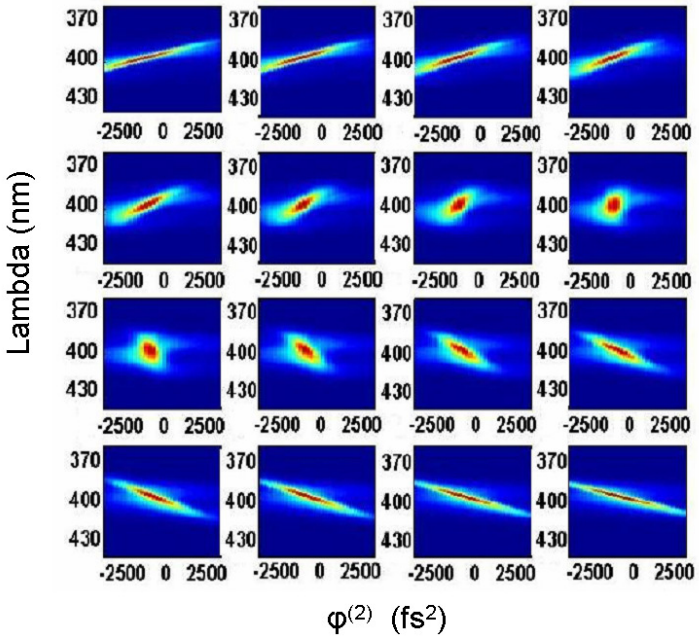

Figure 6.14: Evolution of the SH spectrum (y axis 370 nm<λ<430 nm) function of $\varphi^{(2)}$ (x axis $\pm 2500 fs^2$) for different fixed values of $\varphi^{(3)}$ ($\pm 35000 fs^3$). This graph needs to be read following the lines from the top two the bottom (like a text). The first figure on the left of the first line (figure 1) corresponds to $\varphi^{(3)} = -35000 fs^3$. The second figure of this line (figure 2) corresponds to $\varphi^{(3)} = -30625 fs^3$. Between each figure there is a fixed increment of the third order spectral phase $\varphi^{(3)} = +4375 fs^3$. The last figure on the right of the last line (figure 16) corresponds to $\varphi^{(3)} = 35000 fs^3$.

6.3.2 Theoretical introduction

The starting point of this analysis is the equation:

$$I_B(\omega) \propto \frac{I_A(\omega)^3}{|\phi''(\omega)|^2} \tag{6.3}$$

that has been derived for XPW generation using the stationary phase approximation. This formula, valid for sufficiently chirped pulses ($|\phi''(\omega)| > 1/\Delta\omega^2$, $\Delta\omega$ spectral bandwidth), states that the intensity of the spectrum of the cross-polarized wave $I_B(\omega)$ can be linked to the intensity of the spectrum of the fundamental pulse $I(\omega)$ and its spectral phase second order derivative $\phi''(\omega)$. The corresponding expression for second harmonic generation is:

$$I_{SHG}(2\omega) \propto \frac{I^2(\omega)}{|\phi''(\omega)|} \tag{6.4}$$

The validity of (6.4) can be confirmed by recording the SHG spectrum of a near Fourier-transform limited pulse to which a purely parabolic phase $\varphi^{(2)}(\omega - \omega_0)^2/2$ is added. In this case, the asymptotic expression of the SHG spectrum is a hyperbolic function of the second order phase $\varphi^{(2)}$ since the expected SHG spectrum is, according to (6.4):

$$I_{SHG}(2\omega) \propto \frac{I^2(\omega)}{\varphi^{(2)}} \tag{6.5}$$

Fig. 6.15 shows some typical experimental SHG signal recorded, at a given pulsation, as a function of the second order phase. A Lorentzian fit confirms the validity of (6.4), hyperbolic at large chirps.
When a set of purely linear chirps, $\varphi^{(2)}$, is added to the the spectral phase, $\varphi(\omega)$, of an input pulse, the total spectral phase becomes $\phi(\omega) = \varphi(\omega) + \varphi^{(2)}(\omega - \omega_0)^2/2$ and equation (6.4) predicts, for a given frequency, symmetric and hyperbolic decays of the SHG intensity with large positive and large negative $\varphi^{(2)}$ values, these decays being symmetric with respect to $\varphi''(\omega)$. The algorithm consists in finding the optimal hyperbolic fit at large chirps and returning, for every frequency, the value of $\varphi''(\omega)$ (the local chirp). The pulse spectral phase is then retrieved by a double integration.

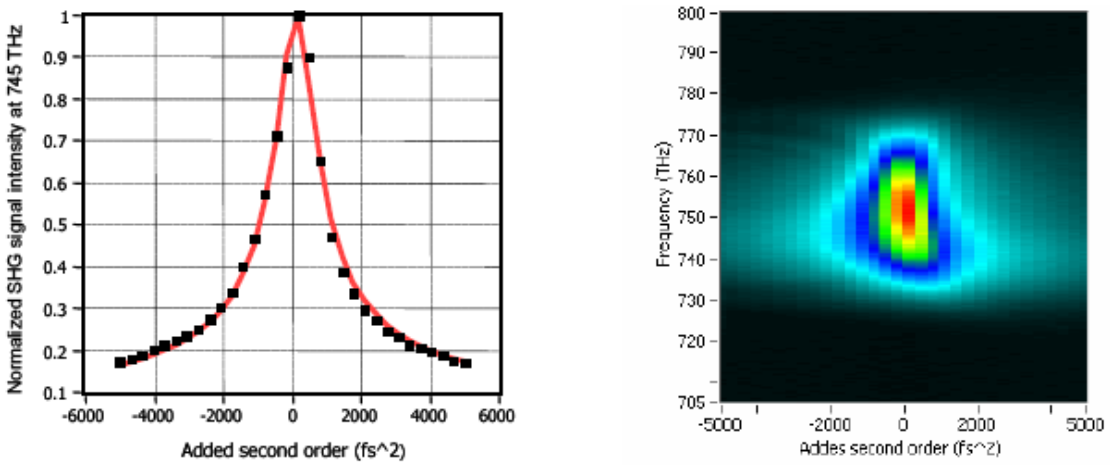

Figure 6.15: Left:typical Lorentzian fit (solid line) to the experimental data (dotted line)at a given wavelength. Right: map of the SHG spectra as function of frequency and added second order phase coefficient.

6.3.3 Examples

To illustrate the efficiency and accuracy of this method I have simulated the SHG spectrum obtained for a chirp scan from $-3000fs^2$ to $+3000fs^2$ for four different input pulses:
- Fourier transform (6.16.a),
- pure second order phase of $+1000fs^2$(6.16.*b*),
- pure third order phase of $+50000fs^3$(6.17.a)
- sinusoidal phase (6.17.b).

The pictures also show the fitted value of $\varphi''(\omega)$ (the local chirp) with a white dotted line. In

the case of a pure second order phase, $\varphi''(\omega) = const$; the constant giving the value of the initial chirp. For the purely third order spectral phase pulse, the image corresponds to linear chirp optimization vs wavelength, as the local chirp of a third order is linear. For a more complex phase, the image is distorted but still gives for each wavelength the local chirp.

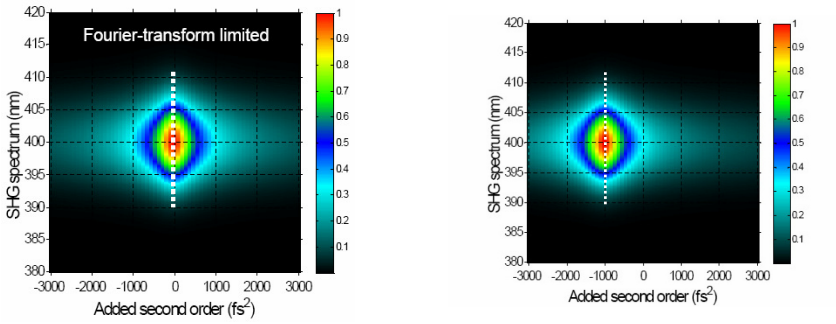

Figure 6.16: SHG spectrum obtained for a chirp scan from $-3000fs^2$ to $+3000fs^2$ for a Fourier transform limited input pulse (a), for an input pulse with a pure Chirp (b)

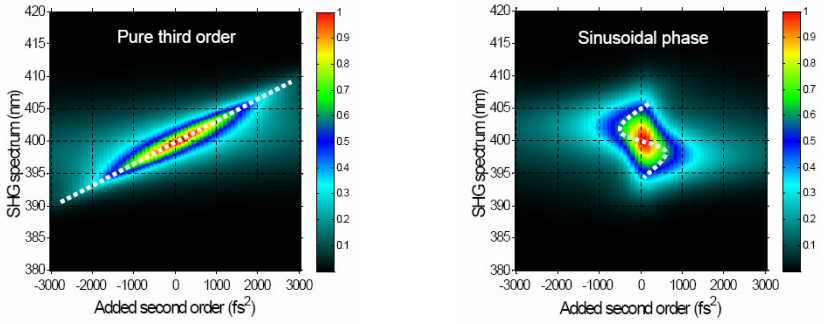

Figure 6.17: SHG spectrum obtained for a chirp scan from $-3000fs^2$ to $+3000fs^2$ for an input pulse with pure third order (a), and for an input pulse with a SPM oscillatory phase (b)

6.3.4 Experimental results

In the previous section it is demonstrated theoretically how the spectral phase can be measured using a $\varphi^{(2)}$ scan. This scan is experimentally done with an AOPDF. This measured phase can then be automatically compensated with the same AOPDF. Therefore, both phase measurement and correction are done in a single AOPDF. This closed-loop optimization has been implemented for the first time in the the "salle noire" laser system. I have previously shown that, due to the small stretching factor, the B integral of this source is quite high (B > 3). I now demonstrate that the AOPDF can be used to measure the spectral phase induced by SPM and then compensate for the measured phase distortion. For the pulse measurement, a small fraction of the output energy (< 1 μJ) is selected with a beam splitter and focused with a f=500 mm focal length lens into a 50 μm type-I BBO crystal. The generated SHG is separated from the fundamental and collected with a commercial spectrometer (AvaSpec-3648 from Avantes). Fig. 6.18a,b and Fig. 6.19c,d show the SHG spectra versus chirp traces together with the extracted local chirp function (white line) for four states: initial state at low energy (Fig. 6.18a),

optimized pulse at low energy (Fig. 6.18b), pulse at high energy with the same phase settings (Fig. 6.19c), optimized pulse at high energy (Fig. 6.19d).

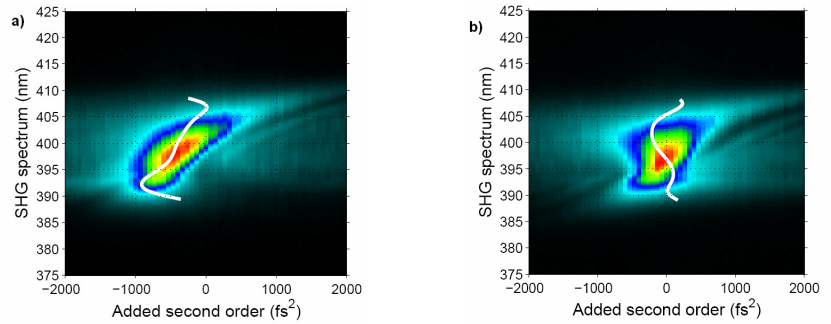

Figure 6.18: Chirp scan of a non compressed pulse (a), Chirp scan after optimization of the polynomial phase (b)

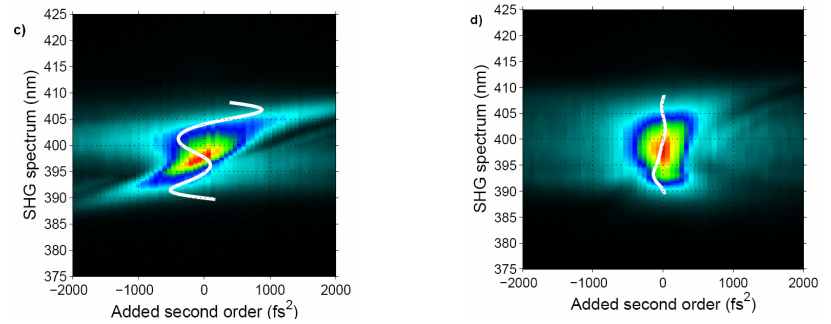

Figure 6.19: Chirp scan under the same conditions then Fig. 6.18b but with increased seed energy into the second amplifier (c), Chirp scan after correction of the nonlinear phase at high energy (d)

Fig. 6.18a shows an input spectral phase mainly dominated by a residual second and third order spectral phase resulting from imperfect optimization of the compressor. This phase is automatically compensated after a polynomial fit to the third order. The resulting trace after this compensation is shown in Fig. 6.18b. From this measurement it is visible that the remaining phase is oscillatory and can not be fitted with a low order polynomial. Fig. 6.19c clearly indicates that, changing the seeding of the second amplifier from 600 to 900 μJ, dramatically changes the spectral phase of the amplified pulses, in particular increasing the amplitude of the oscillations of the local chirp. Due to the small stretching of our pulse (10 ps) the B-integral of our laser system is estimated to be about 4-5 rad for the high energy seed. When a pulse is sufficiently chirped as in a CPA stretcher, the temporal profile corresponds to the spectral profile and so the nonlinear phase corresponds to the the spectral shape: $\varphi_{nl} \propto n_2 I(t) \propto n_2 I(\omega)$ (where $I(\omega)$ is typically a Gaussian). When we compensate the polynomial spectral phase of the stretcher/compressor pair the residual phase comes from nonlinear effects in the amplification crystal and the local chirp is then the second order derivative of a Gaussian function. This correspond to the oscillatory trace measured in Fig. 6.18b, Fig. 6.19c. In particular at high energy there is a large oscillation of period 50nm (12.5nm on the SHG

spectrum) with amplitude of about $\pm 900 fs^2$. As predicted theoretically in [1], this phase can be pre-compensated numerically with the pulse shaper. Naturally this assumes that the non linear phase is small compared to the stretching factor and this is still valid in our case. Fig. 6.19d shows experimentally the effect of the pre-compensation. The residual phase measured after optimization is less than 0.5 rad which corresponds to the typical measurement precision of SPIDER[3] or FROG[4] devices. The pulse temporal duration, measured with an home made SPIDER, is shown in Fig. 6.20.

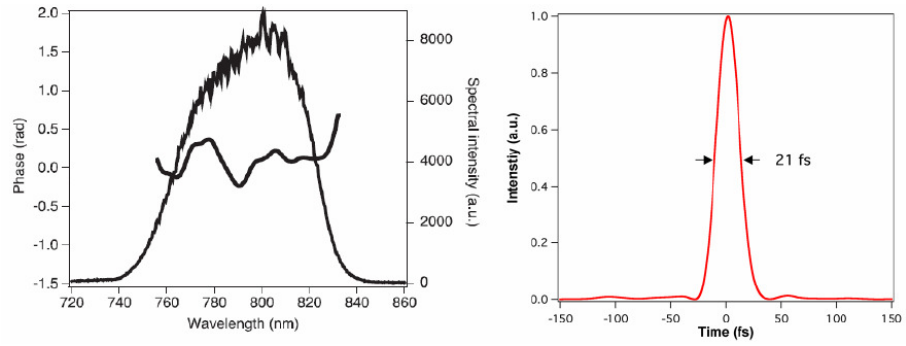

Figure 6.20: Temporal measurement and spectrum and phase after DazScope optimization.

6.3.5 Discussion

Compared to standard pulse measurement technique like FROG or SPIDER, the DazScope technique is a phase-only method and strictly speaking, is not a pulse measurement technique. For example a double structure pulse will not be measured. As a phase-only technique it can be compared to the Multiphoton Intrapulse Interference Phase Scan (MIIPS) [2, 5, 6, 7]. The DazScope technique is really adapted for the characterization and optimization of the output pulses of a CPA laser where an AOPDF is present. In these cases it has several advantages: the traces are very visual and in particular any residual linear chirp translates to a relative shift to the zero added second order phase. There is no ambiguity on the sign of this chirp. This technique is also very sensitive to the high order terms of the spectral phase. We have seen previously how it has been used for measuring and pre-compensating the non linear phase induced by SPM during amplification. We have also discussed in the introduction how the residual spectral phase affects the temporal quality of pulses at the output of a CPA laser and is responsible for the coherent (ps) contrast. Finally the measuring setup is extremely simple consisting of just a BBO crystal and the spectrometer. It can be placed as close as possible to the experiment even inside the interaction chamber.

Bibliography

[1] A. Braun, S. Kane, and T. Norris. Compensation of self-phase modulation in chirped-pulse amplification laser systems. *Opt. Lett.*, 22(9):615–617, 1997.

[2] Y. Coello, V. V. Lozovoy, T. C. Gunaratne, B. Xu, I. Borukhovich, C. Tseng, T. Weinacht, and M. Dantus. Interference without an interferometer: a different approach to measuring, compressing, and shaping ultrashort laser pulses. *J. Opt. Soc. Am. B*, 25(6):A140–A150, 2008.

[3] C. Iaconis and I.A. Walmsley. Spectral phase interferometry for direct electric-field reconstruction of ultrashort optical pulses. *Opt. Lett.*, 23(10):792–794, 1998.

[4] B. Kohler, V. V. Yakovlev, K. R. Wilson, J. Squier, K. W. DeLong, and R. Trebino. Phase and intensity characterization of femtosecond pulses from a chirped-pulse amplifier by frequency-resolved optical gating. *Opt. Lett.*, 20(5):483–485, 1995.

[5] V. V. Lozovoy, B. Xu, Y. Coello, and M. Dantus. Direct measurement of spectral phase for ultrashort laser pulses. *Opt. Express*, 16(2):592–597, 2008.

[6] I. Pastirk, Bojan Resan, Alan Fry, John MacKay, and M. Dantus. No loss spectral phase correction and arbitrary phase shaping of regeneratively amplified femtosecond pulses using miips. *Opt. Express*, 14(20):9537–9543, 2006.

[7] I. Pastirk, X. Zhu, R. M. Martin, and M. Dantus. Remote characterization and dispersioncompensation of amplified shaped femtosecondpulses using miips. *Opt. Express*, 14(19):8885–8889, 2006.

6.4 CEP

Up to now I have demonstrated the generation of 4 mJ, 21 fs pulses at 1 kHz. I have also presented how the pulses at the output of the oscillator are CEP stabilized. This is not enough for having CEP stable pulses at the output of the laser. All the optical elements after the oscillator introduce some phase fluctuations $\Delta\varphi_0$. The fluctuations in the multi-pass amplifier are caused by variations of the non linear index of the crystal. These variations are induced by fluctuations in the intensity of the pulses due to the fluctuations of the pump intensity. The CEP fluctuations in the strecther/compressor originate from dispersion fluctuations caused for example by a variations of beam pointing or beam path. The CEP noise thus originates from the oscillator, laser amplifiers and the compressor. In particular the main contribution comes from the oscillator. In the oscillator the repetition rate is 80 MHz compared to the kHz of the amplified pulses. There is therefore an accumulation of the variations of $\Delta\varphi_0$ over a period of 1 ms. In conclusion, to build a CEP stabilized system, it is necessary to have:

- a device for fixing the value $\Delta\varphi_0$. This is realized using two wedges inside the oscillator cavity. These wedges can be finely moved.
- a first feedback loop after the oscillator for actively stabilizing $\Delta\varphi_0$.
- a second feedback loop just at the end of the laser chain.

Although the measurement of $\Delta\varphi_0$ for the both loops is based on nonlinear interferometry, they are different because the first uses MHz low energy pulses from the oscillator and the second uses the amplified high energy, kHz pulses. The first loop is called fast loop and the second is called slow loop. In the commercial Menlo-system the two feedback loops generate two error signals that are treated to generate a single error signal. The feedback control is based on the modulation of the non linear dispersion of the Ti:Sa crystal of the oscillator. This is tuned by changing the intensity of the pump laser with an acousto-optical modulator. I have already discussed the scheme for measuring $\Delta\varphi_0$ after the oscillator (section 2.2.1). I now present the setup for measuring the slow changes of the CEP. This device is named an f-2f interferometer. The schematic is reported in Fig. 6.21. A beam splitter selects low energy pulses that are focused in a sapphire plate. This step is needed for broadening the spectrum to one octave. They are then focused on a BBO crystal, phase matched for converting the infrared side of the spectrum. The SHG and the fundament signal are cross-polarized and have a certain delay τ_0. These two signals pass then through a polarizer with the transmission axes at 45 degrees compared to the polarization signal of the two beams to make them interfere. The signal measured with the spectrometer presents many spectral fringes (Fig. 6.22). The CEP drift is extracted by the shift of these fringes as a function of time. In particular the spectrometer signal is given by the equation:

$$I(\omega) \propto \left| \int_{-\infty}^{+\infty} [E_F(t+\tau_0) + E_{SH}(t)]\, exp(-i\omega t) dt \right|^2 \tag{6.6}$$

that can be expressed in the form:

$$I(\omega) \propto I_F(\omega) + I_{SH}(\omega) + 2\sqrt{I_F(\omega)I_{SH}(\omega)}cos\left[((\varphi_0 + \Phi_{SH}(\omega) - \Phi_F(\omega) + \omega\tau_0)\right] \tag{6.7}$$

where $I_F(\omega)$ and $I_{SH}(\omega)$, ($\Phi_{SH}(\omega)$ and $\Phi_F(\omega)$) are the respective spectral intensity (spectral phases) of the fundamental and the SH. φ_0 is the input CEP phase. The argument of the cosine is extracted with the Fourier Transform Spectral Interferometry (FTSI) algorithm. As it was presented in the case of a SPIDER measurement this algorithm consists of making a Fourier transform to get into the time domain, to apply a band pass filter around τ_0 and to make another Fourier transform back in the frequency domain. It is then possible to measure the CEP variation between successive pulses. A tension signal proportional to the CEP variation is then sent to the acousto-optic RF driver for the CEP stabilization.

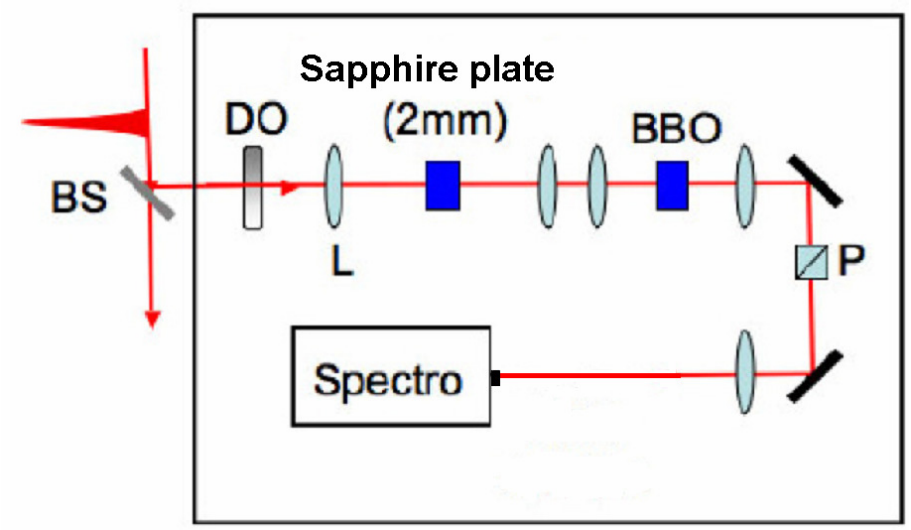

Figure 6.21: f-2f interferometer for measuring the CEP shift of the pulses at the output of the laser chain